

# EFFICIENCY OPTIMIZATION OF AN OPEN- LOOP CONTROLLED PERMANENT MAGNET SYNCHRONOUS MOTOR DRIVE USING ADAPTIVE NEURAL NETWORKS

*Munaf S. N. Al-Din, PhD, Assistant Prof.*

Department of Electrical and Computer Engineering, College of Engineering  
and Architecture, The University of Nizwa, Nizwa, Sultanate of Oman

*Majid A. Al-Tae, PhD, Prof.*

School of Computing and Information Systems,  
Kingston University, London, UK

---

## Abstract

When a Permanent Magnet Synchronous Machine (PMSM) is utilized for applications where high dynamic performance is not a requirement, a simple open loop control strategy can be used to control them. PMSMs however are prone to instability when operated open loop in a variable speed drive, particularly at mid-frequencies/speeds. This paper presents an open-loop control strategy based on a direct adaptive neural network controller is developed for efficiency optimization of open-loop controlled PMSM drive. Stability constraints of the drive system which was previously reported are used to maintain both stable and highly efficient operation of the drive system. The adopted neural network can be viewed as a method for nonlinear adaptive system identification, relying on pattern recognition of stability limits and maximum obtainable efficiency. Results from computer simulation show that a stable and highly efficient operation can be maintained for the drive system under study irrespective of load and supply variations. The obtained results are also found in correlation with previously reported experiments and observations.

---

**Keywords:** Adaptive Neural networks, variable speed drive, PM synchronous motor, open loop control, stability analysis, efficiency optimization

## 1. Introduction

In the last 20 years Permanent Magnet Synchronous Machine (PMSM) are becoming more indispensable in many industrial applications.

The PMSM is superior to both induction motor drives and DC motor drives because of the inherent advantages of these motors include high efficiency, high power factor, high power density, easy maintenance, fast dynamic response, and the minimum magnet cost because of low magnet weight requirement. Among the PMSM drives the interior permanent magnet synchronous motor (IPMSM) has gained much attention and has become the most used drive in machine tool servos and modern speed control applications (D. W. Novotny 1996) (W. Leonhard 1996). With permanent magnets buried inside the rotor, features such as smooth rotor surface and reduced air-gap will results in permitting higher speed with quiet operation and better dynamic performance. Furthermore, IPMSMs possess low torque ripples, self-commutation over a wider speed range, more efficient use of the volume of the machine and the ease with which it can be controlled (Binns, K.J. 1984).

Because of magnetic circuit saliency, certain current control method can be applied to this motor for enhancing its efficiency, torque and reducing its overall current. For rapid torque build-up which is required by variable speed and fast dynamic response drives, current can be controlled by several methods, such as hysteresis, ramp comparison, and predictive current control schemes (P. Vas 1998). However, like any other ac machine, the IPMSM is inherently nonlinear multivariable coupled system with high order complex dynamics (Faa-Jeng Lin 2004). This results in parametric uncertainties in the dynamic model, and this necessitates the need for advanced robust control techniques. A number of control methodologies were proposed to control IPMSM, such as vector or field oriented method (Stefan Soter 2005), direct torque method (Yong Liu 2005), nonlinear control (B. Zhang 2000), adaptive control (S. R. Bowes 2000), robust control (H. Z. Akpolat 2000), and variable structure control (S. K. Chung 1995). In these control schemes, the speed or position signal is necessary for establishing the outer speed loop feedback and also in the flux and torque control algorithms, and hence they are classified to be a closed loop controllers. In contrast to the mentioned methods, a hybrid rotor design allows open-loop control from an inverter without rotor position feedback. This simple control method is suggested to replace conventional induction motors in applications like fans, pumps and ventilation systems where high dynamic performance is not a requirement (Perera, P. D. 2003) (Al-Taee, M.A. 2004) (Al-Taee, M.A. 2006). A precise speed control and improved efficiency can therefore be achieved without changing the drive control hardware since the only connections made to the machine are those of the three-phase supply from the inverter. However, unlike the close loop control drives, the open loop controlled PM synchronous motor drives have received limited attention over the past years. This was mainly due to instability problems in these PM synchronous motors

under the open-loop control approach (Mellor, P.H. 1988) (Mellor, P.H. 1991) (Shimmin, D.W. 1995).

Several control methods were proposed and implemented to optimise the efficiency of PM synchronous motor drives. The copper loss in surface PM motor drives was minimised by attaining a maximum torque-per-ampere current ratio (Morimoto, S. 1990). The existence of core loss in this type of machines causes this optimum to deviate from the unity power factor condition, especially for high-speed operation (Al-Tae, M.A. 2004). Another approach to optimal efficiency includes two loss minimisation strategies the loss-mode control and the search control (Colby, R.S. 1988) (Mademlis, C. 2004) (Cavallaro, C. 2005). However, efficiency optimization controllers require both a good dynamic model of the system and knowledge of inaccuracies and uncertainties in the model. Adaptive control is an attractive approach considering the uncertain and time varying parameters in IPMSM. Neural networks are now considered one of the most important tools in developing adaptive controllers since they have important features that overcome the typical difficulties in designing control systems. For instance, the dynamics of the motor need not be completely known as a prior condition for controller design. This is very desirable for a drive system to have since the dynamic characteristics of motor change with configuration and it is impossible to consider all the effects from disturbances. Also, the ability of these networks for adaptation and disturbance rejection and their highly parallel nature of computation make this approach suitable for real-time applications.

The objective of this paper is to investigate the stability boundaries of a previously reported drive system (Mellor, P.H. 1991) with the aim of improving its efficiency by means of a control algorithm based on the Liapunov stability method and an adaptive neural network (ANN). Real-time computed stability boundaries are fed to a neural network controller, which adaptively maintains both stable and highly efficient operation of the drive system. The suggested open loop control method has excellent potential for applications in industrial environments, where a precise speed control and improved efficiency want to be achieved efficiently and without changing the drive control hardware.

## **2. Drive system description**

The PMSM machine used in the drive has an asymmetrical buried-magnet rotor is shown in Figure 1. The stator has a four-pole winding within a D60 frame and has a continuous torque rating of 3 N.m. The constructional details of the IPMSM machine are given in Table 1 while other parameters are listed in Appendix II.

Table 1. PMSM constructional parameters.

Parameter	Value
Number of phases	3
Magnet material	SmCo <sub>5</sub>
Rotor diameter, mm	79
Axial length, mm	70
Motor inertia, J	$0.25 \times 10^{-3} \text{ kg.m}^2$
Motor viscous friction, D	$0.03 \times 10^{-3} \text{ kg.m}^2.\text{s}^{-1}$

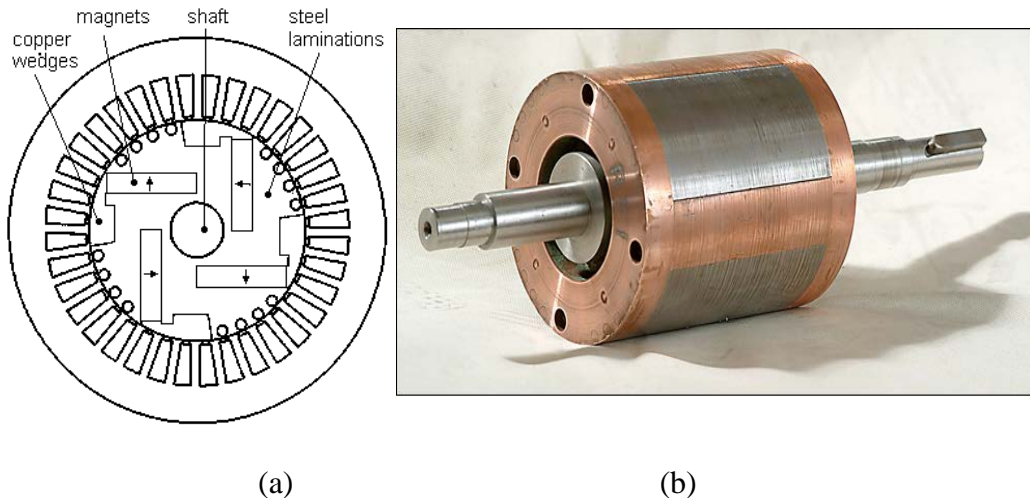


**Figure 1:** Permanent magnet rotor (a) Rotor cross sectional view (b) Complete prototype rotor.

### 3. Drive system model

The drive system model consists of two major components, the inverter and the PM synchronous motor. An ideal three-phase voltage source and a series resistance model is considered adequate for both the steady state and dynamic performance of the inverter used in the drive system under investigation. The equivalent circuit of the PM motor (Mellor, P.H. 1991) (Shimmin, D.W. 1995) (Yang Yi 2003) (Al-Tae, M.A. 1995) shown in Fig. 2a, is combined with the inverter equivalent circuit shown in Fig. 2b to give the complete equivalent circuit of the drive system. The drive equivalent circuit is further reduced to a simple Thevenin form as shown in Fig. 2c; (Al-Tae, M.A. 2006) (Mellor, P.H. 1988) (Mellor, P.H. 1991) (Al-Tae, M.A. 1995). The influence of rotor cage bars on the machine operation is assumed to be negligible in the present work.

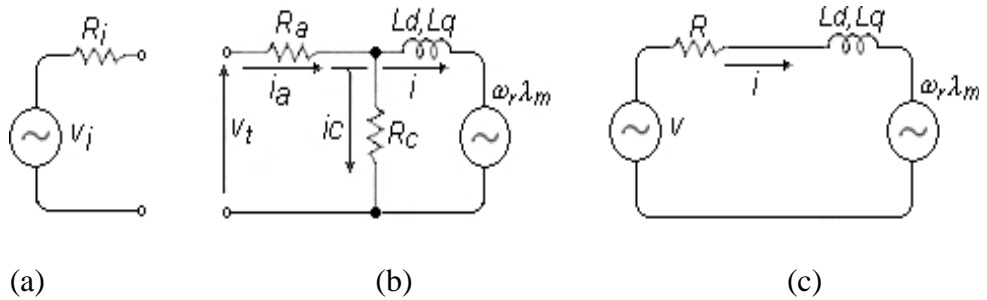


**Figure 2:** Electrical Equivalent circuits (a) Inverter (b) Permanent magnet motor (c) Drive system

The dynamics of the drive system is written in terms of the following non-linear differential equations which represent the first-order dynamics of the drive system:

$$\frac{d\delta}{dt} = \omega_s - \omega_r \tag{1}$$

$$J \frac{d\omega_r}{dt} = 1.5 p^2 [\lambda_m i_q + (L_d - L_q) i_q i_d] - D \omega_r - pT_L \tag{2}$$

$$L_d \frac{di_d}{dt} = -R i_d + L_q i_q \omega_r - v \sin(\delta) \tag{3}$$

$$L_q \frac{di_q}{dt} = -R i_q + L_d i_d \omega_r - \lambda_m \omega_r + v \cos(\delta) \tag{4}$$

Derivation of the linearised equations and parameters of the drive system under study is well discussed in references (Al-Tae, M.A. 2006) (Mellor, P.H. 1988) (Mellor, P.H. 1991). Letting  $x_1, x_2, x_3,$  and  $x_4$  denote the torque angle ( $\delta$ ), rotor velocity ( $\omega_r$ ), and direct and quadrature axes currents  $i_d$  and  $i_q$  respectively, the linearised drive model can be written as:

$$\dot{\mathbf{x}} = \mathbf{f}(\mathbf{x}, \mathbf{u})$$

$$\mathbf{x} = [\delta, \omega_r, i_d, i_q]^T \tag{5}$$

$$\mathbf{u} = [\omega_s, v, T_L]^T$$

where  $[\mathbf{x}]$  and  $[\mathbf{u}]$  are the state-space vector and input-control vector respectively, and  $f([\mathbf{x}], [\mathbf{u}])$  is a nonlinear function of  $[\mathbf{x}]$  and  $[\mathbf{u}]$ . Letting  $\mathbf{A}$  denotes the Jacobean matrix of  $f$  with respect to  $\mathbf{x}$  at  $\mathbf{x} = 0, \mathbf{u} = 0$  and  $\mathbf{B}$  denotes the Jacobean matrix of  $f$  with respect to the same point, the linearisation of the original nonlinear system at the equilibrium point (0) is given by:

$$\dot{\mathbf{x}} = \mathbf{Ax} + \mathbf{Bu} \tag{6}$$

The above Taylor expansion starts directly with the first-order term, due to the fact that  $f(0) = 0$ . The system matrix  $\mathbf{A}$  of Eqn. 6 are given by:

$$\mathbf{A} = \begin{bmatrix} 0 & -1 & 0 & 0 \\ 0 & -\frac{D}{J} & \frac{3p^2}{2J}(L_d - L_q)x_4 & \frac{3p^2}{2J}[\lambda_m + (L_d - L_q)x_3] \\ -\frac{v \cos x_1}{L_d} & \frac{L_q}{L_d}x_4 & -\frac{R}{L_d} & \frac{L_q}{L_d}x_2 \\ -\frac{v \sin x_1}{L_q} & -\frac{(\lambda_m + L_d x_3)}{L_q} & -\frac{L_d}{L_q}x_2 & -\frac{R}{L_q} \end{bmatrix} \quad (7)$$

The dynamic parameters of the A and B matrices under various operating conditions are obtained from the drive inputs of torque, frequency and voltage. The method of finding these parameters is based upon an iterative analysis of the drive equivalent circuit given in Fig. 2. The magnetic parameters used in this model, namely the permanent magnet flux  $\lambda_m$ , the direct axis inductance  $L_d$  and the quadrature axis inductance  $L_q$ , must be adjusted to reflect the changing condition of saturation. The complex nature of the field distribution within the rotor means that significant variations will exist in all three parameters. These are summarised by the following dependencies on the direct and quadrature components of the armature currents  $i_d$  and  $i_q$ :

- (i)  $L_d$  varies with  $i_d$ ,
- (ii)  $L_q$  varies with  $i_q$  and
- (iii)  $\lambda_m$  varies with  $i_q$ .

The model parameters and their variation were measured from extensive load testing of the permanent magnet motor. The measurement procedure was previously reported in references ; (Al-Tae, M.A. 2006) (Mellor, P.H. 1988) (Mellor, P.H. 1991) (Al-Tae, M.A. 1995), from which the following expressions were derived:

$$L_q = L_{q0} - K_q i_q \quad (9)$$

$$L_d = \begin{cases} L_{d0} - K_{d1} i_d, & i_d \geq 0 \\ L_{d0} - K_{d2} i_d, & i_d < 0 \end{cases} \quad (10)$$

$$\lambda_m = \begin{cases} \lambda_{m0}, & i_q \leq I_{qe} \\ \lambda_{m0} - K_e (i_q - I_{qe}), & i_q > I_{qe} \end{cases} \quad (11)$$

The elements of system matrix A which vary with drive inputs of torque, frequency and voltage are obtained from Eqns. 9 - 11 while other parameters given in Appendix II. It was shown that these techniques give accurate estimate of the steady state performance of the drive under consideration over a wide range of frequencies, torques, voltage, and power factors.

#### 4. Stability Analysis

The open loop stability characteristics of the drive under consideration have been previously analysed with and without taking into account the effect of cage bars on the machine operation, (Al-Tae, M.A. 2004) (Mellor, P.H. 1991) (Shimmin, D.W. 1995). From analysis based on the eigenvalues of matrix A, it was demonstrated that machine operation with lagging power factor remains more stable than with leading power factors. The type of machine used in the drive can also operate at leading power factor but only within a limited frequency range. A control strategy, which is restricted to a constant value of 0.9 lag, was therefore suggested (Mellor, P.H. 1991) to maintain the machine stable over the full working range of torques and frequencies. For maximum efficiency however it is necessary to run the machine at power factors closer to unity (Binns, K.J. 1984) (Al-Tae, M.A. 2004). With the fast determination of stability boundaries, machine operation at power factors closer to unity then becomes possible to be implemented in real-time.

Liapunov linearisation method is concerned with local stability of the nonlinear system. It formalises the intuition that a nonlinear system behaves similar to its linearised approximation for a small range of motion around a nominal operating point. Using this method, the stability properties can be tested by a scalar function  $V(x)$ , which indirectly reflects the magnitude of system state vector (Takahashi, Y. 1972) (Slotine, J.-J.E 1991). There is no general method of determining the function  $V(x)$  for a nonlinear system. All attempts to determine a suitable Liapunov function for the system equations presented in Appendix I were unsuccessful. The nonlinear state equations of the drive system are therefore linearised by using the procedure described in section 3. Liapunov method is then applied to the resulting linear time-invariant (LTI) system. This approach is justified since the stability of the nonlinear system is of local interest. A possible Liapunov's function for the LTI system of Eqn. (2) can be described by:

$$V = \mathbf{x}^T \mathbf{P} \mathbf{x} \quad (12)$$

where P is a 4×4 real symmetric matrix. Differentiating the positive definite function (V) of Eqn. (12) along the system trajectory yields the following quadratic form (Slotine, J.-J.E 1991) (Franklin, G.F. 1994):

$$\dot{V} = \dot{\mathbf{x}}^T \mathbf{P} \mathbf{x} + \mathbf{x}^T \mathbf{P} \dot{\mathbf{x}} = -\mathbf{x}^T \mathbf{Q} \mathbf{x} \quad (13)$$

where Q is defined by

$$\mathbf{A}^T \mathbf{P} + \mathbf{P} \mathbf{A} = -\mathbf{Q} \quad (14)$$

In Eqn. (14), the matrix P is computed from the system matrix A (Eqn. 7) and a selected positive definite matrix Q (the identity matrix I). For a strictly stable LIT system, it is necessary and sufficient that the unique matrix P solution of Eqn. (14) be symmetric positive definite. Applying

Sylvester’s criterion, where all successive principal minors should be positive, tests the positive definiteness of P, i.e.

$$\text{MINR}_1 > 0, \text{MINR}_2 > 0, \text{MINR}_3 > 0, \text{ and } \text{MINR}_4 > 0 \quad (15)$$

The principal minors of Eqn. (15) are computed from the obtained elements of matrix P, as follows:

$$\text{MINR}_1 = P_{11} \quad (16)$$

$$\text{MINR}_2 = P_{11} P_{22} - P_{12}^2 \quad (17)$$

$$\text{MINR}_3 = [P_{11}(P_{22}P_{33} - P_{23}^2) + P_{13}(P_{12}P_{23} - P_{22}P_{13}) - P_{12}(P_{12}P_{33} - P_{13}P_{23})] \quad (18)$$

$$\text{MINR}_4 = \left[ \begin{aligned} &P_{11}(P_{32}m_1 - P_{23}m_2 + P_{24}m_3) - P_{12}(P_{12}m_1 - P_{23}m_4 + P_{24}m_5) \\ &+ P_{13}(P_{12}m_2 - P_{22}m_4 + P_{24}m_6) - P_{14}(P_{12}m_3 - P_{22}m_5 + P_{23}m_6) \end{aligned} \right] \quad (19)$$

and

$$m_1 = P_{33}P_{44} - P_{34}^2 \quad (20)$$

$$m_2 = P_{23}P_{44} - P_{34}P_{24} \quad (21)$$

$$m_3 = P_{23}P_{34} - P_{33}P_{24} \quad (22)$$

$$m_4 = P_{13}P_{44} - P_{34}P_{14} \quad (23)$$

$$m_5 = P_{13}P_{34} - P_{33}P_{14} \quad (24)$$

$$m_6 = P_{13}P_{24} - P_{23}P_{14} \quad (25)$$

The results from computer simulation indicate that the first principal minor (Minor-1) of Liapunov function is of a distinct sign change whereas other principal minors (Minor-2 – Minor-4) remain positive in the region of interest. The rate of change of Minor-2 – Minor-4 with respect to the input voltage can be used to define boundaries of instability. The system is stable if the rate of change is positive and it is unstable if the rate of change is negative.

Figure 3 shows an example of the obtained results that illustrates the behaviour of Liapunov minors (Minor-1 - Minor-4) at a supply frequency of 50 for a range of changes in: supply voltage (0.9 - 1.2.) per unit voltage, load torques (1 – 3), and for different rotational directions. A similar order of results is also obtained for other supply frequencies. The minimum supply voltage below which the system is definitely unstable can be defined by the condition, at which Minor-1 changes its sign from positive to negative,

$$\text{Minor-1} = 0 \begin{matrix} \uparrow \\ \downarrow \end{matrix} \quad (26)$$

The relatively small computation time for Minor-1 offers the possibility of using Minor-1 as a real-time stability index. The stability boundaries obtained from computer simulation are found in agreement with the previously reported observations and experiments.

### 5- Neural Network Optimal Efficiency Controller

The control strategy which always drives the system at optimum efficiency except if the stability constraint (Eqn. 26) dictates otherwise is given in details in (Al-Taee 2008). It should be noticed that the behaviour of real-time systems depends on a certain time requirements and any violation of these requirements may damage the overall operation of the system. Time complexity analysis of algorithms involved in real-time systems is therefore represents an essential requirement to ensure satisfactory response. Such analysis decides whether or not the system response will be acceptable. The time taken by this algorithm is the sum of both compilation and processing (or execution) times. However, as the compilation time does not involve in the online operation of the system, the present analysis is limited to the processing time ( $T_p$ ) which can be estimated either analytically or experimentally (Al-Taee 2001). Experimental measurements of ( $T_p$ ) based on a PC system with a Pentium processor 2.0 GHz, 1 GB RAM and Microsoft Windows XP Professional operating system (real-time mode) indicate that the average  $T_p$  for the first principle minor of Liapunov’s function, over the entire range of drive system operation, is approximately 10 ms.

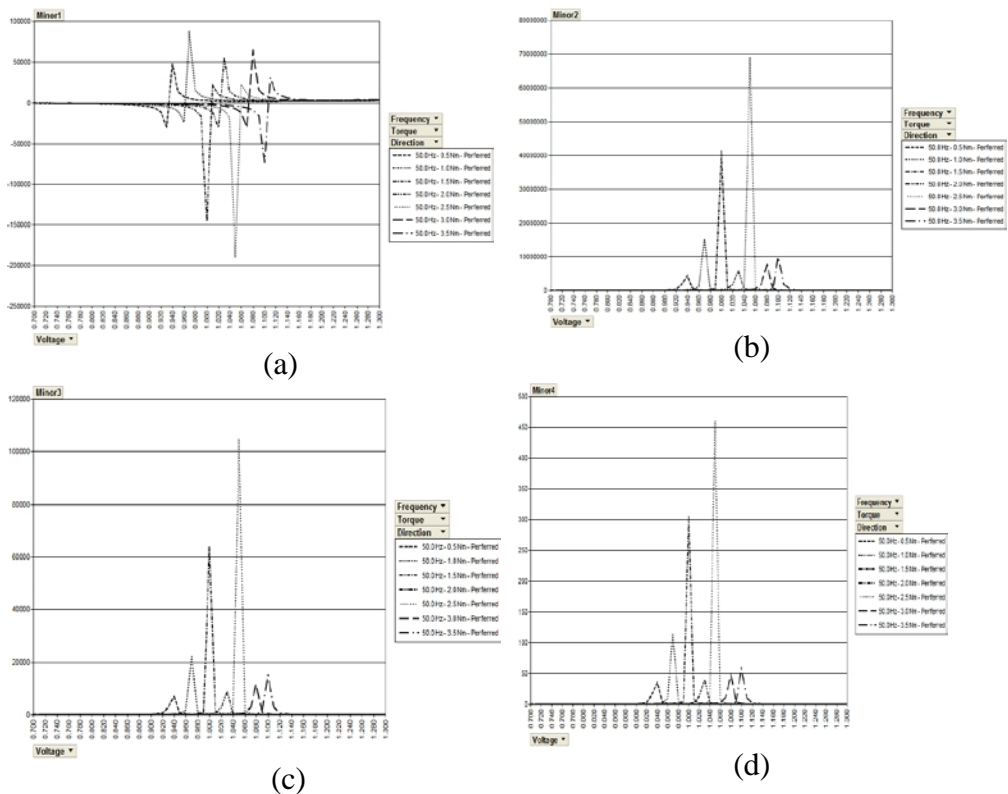


**Figure 3:** Behaviour of Liapunov function minors for different load torques and fixed supply frequency

To overcome the time consuming process in finding the first principle minor of Liapunov’s function, and any possible degraded performance due to parameter variation and module uncertainties; an adaptive ANN estimator/controller is developed to estimate and to maintain optimal stable operating condition for an open-loop PMSM drive. The system is shown in figure 7, and it consists of two three-layer feedforward ANNs; the first ( $N_e$ ) is detected for online identification for the system stability from the knowledge of the torque, frequency and the applied PU voltage; and the function of the second ( $N_p$ ) is to generate the optimal per unit applied voltage for the motor based on the applied torque and frequency.

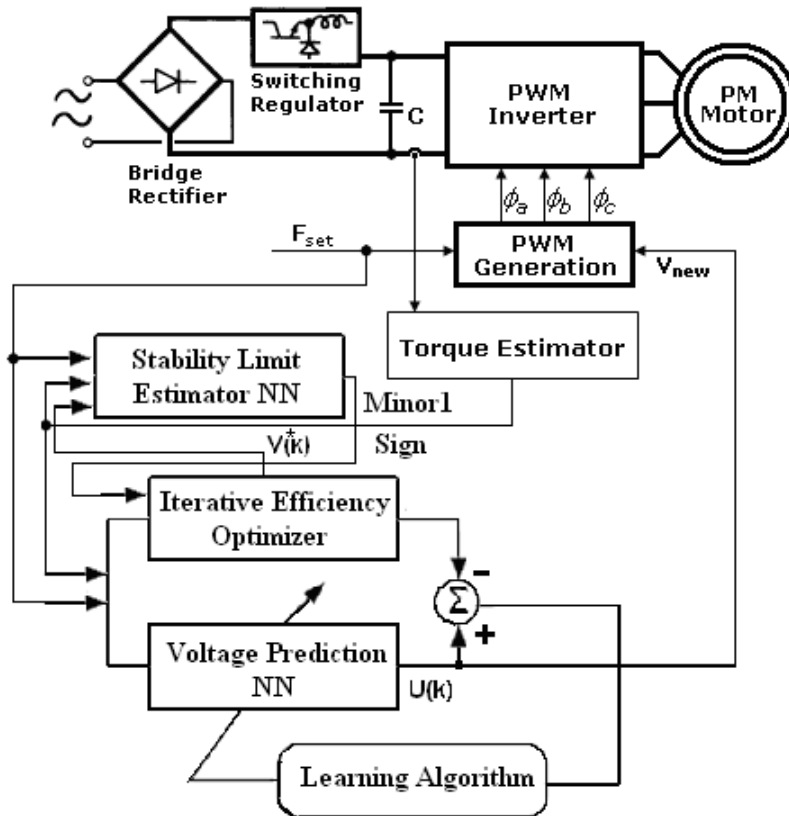


Figure (7): Adaptive neural network efficiency optimizer for PMSM drive.

### 5.1 Stability Limit Estimator NN

The ANN used for the stability limit estimator is a feedforward ANN with three inputs nodes that takes the present torque  $T(k)$ , frequency  $f(k)$ , and the PU voltage  $V(k)$ . The hidden layer has five hidden with an activation function of Tan-sigmoid type, while the output stage has one node has a of Tan-sigmoid activation function. The stability boundaries for the PMSM are identified by presenting a set of input/output patterns to the neural network

and by adjusting its coefficients accordingly through offline learning. Training data are collected from the model described in section 4. Since the change in the sign of the first minor gives an indication for the stability of the system, the authors represent the variation of the first principle minor as ( $\pm 1$ ), thus the output  $y(k)$  after the activation of the output node can only have one value which is either 1 or -1. The batch mode of back-propagation learning is used for offline training purposes, in which neural network update is carried out only after the whole set of the training patterns are presented, based on the gradient descent algorithm.

For initial training of the network the weights are first randomly initialized. With the random values of the weights and biases the output values are compared with the desired values that were gathered from simulated values of the open-loop PMSM. With this comparison, the output layer neurons generate a sum-squared error. The sum-squared error for a set of  $N$  patterns gives the performance index for the network identification which is defined as:

$$P_i = \frac{1}{2} \sum_{n=1}^N (e_i(n))^2 = \frac{1}{2} \sum_{n=1}^N (m_n^i - \hat{m}_n^i)^2 \quad (27)$$

where  $e_i(n)$  is the error of the output layer that is defined by the difference between the actual minor1 sign ( $m$ ) and the estimated one ( $\hat{m}$ ), when the  $i^{\text{th}}$  training pattern is presented.

In order to get the error between the output layers values the weights are continuously updated until the sum-squared error cost function is as small as acceptable for the desired case. The weights are updated to get a minimum error  $E$ , with the use of the gradient descent method. The weight update equation is given by:

$$W_{ij}(k+1) = W_{ij}(k) + \alpha \frac{\partial P_i}{\partial W_{ij}(k)} \quad (28)$$

where  $\alpha$  represents the learning rate,  $W_{ij}(k)$  represents the old weight, and  $W_{ij}(k+1)$  represents the new updated weights. The weights are update through iterations called epochs. The epochs are continued until the error between the actual and output values are as small as desired. The training goal is set to be  $1.0 \times 10^{-8}$  in terms of the performance index  $P_i$ . The obtained performance is value  $1.095 \times 10^{-9}$ , and the network has successfully identified the stability boundaries with the pre-specified accuracy after 80 epochs.

## 5.2 Adaptive Voltage Predictor NN

The neural network adopted for the optimal per unit voltage predictor is a three layers feed-forward neural network with tan-sigmoid/linear

functions. The number of neurons in the hidden layer was chosen heuristically on a trial-and-error basis with random weights. The basic training process employed for this task is shown in Figure 8, where  $r(k)$  represents the inputs, which are the torque and the frequency,  $V(k)$  is the optimal per unit voltage obtained from the iterative efficiency optimizer,  $U(k)$  the predicted per unit voltage by using the Adaptive NN and  $e(k)$  is the difference between the computed and predicted per unit voltages.

As mentioned earlier, the efficiency optimising algorithm is only effective at steady-state condition. Whenever a certain change in the speed command or in the applied load is detected, the efficiency optimisation process is over-ruled to maintain stable operation. This is achieved by overexciting the PM machine through setting the inverter voltage as a function of a predefined V/F ratio ( $V \cong 1.2$  p.u.). This supply voltage is initially set to a predefined V/F ratio which ensures stable operation for the drive system. The voltage is then gradually reduced by the iterative efficiency optimizer with the aim of minimising the total DC power supplied to the drive system. Since the inverter input voltage ( $V_{dc}$ ) is constant, the dc-link current ( $I_{dc}$ ) is used as an indicator for the supplied input power. The controller effort in minimising the input power (or  $I_{dc}$ ) when the drive is operated with light- and full-load conditions is shown in Figure 9. For the light-load condition (Figure 9a), there is no stability restriction and the efficiency optimiser continues its search for the minimum value of  $I_{dc}$  until  $V_{new} = V_{new}(\min)$ . For high loads however the minimum  $I_{dc}$  value cannot be obtained because of the imposed stability constraints. In this case, the efficiency optimisation process is terminated at the stability boundary (i.e, when  $V_{new} = V_{SL}$ , as illustrated in Figure 9b. Further reductions in the voltage command will lead to unstable operation and the PMSM will lose its synchronism. Once the optimal stable condition is reached, which can be identified by using the stability NN, the computed value of the per-unit voltage is compared with that predicted by the Voltage Prediction NN. The error signal  $e(k)$  is defined as:

$$e(k) = V(k) - U(k) \tag{29}$$

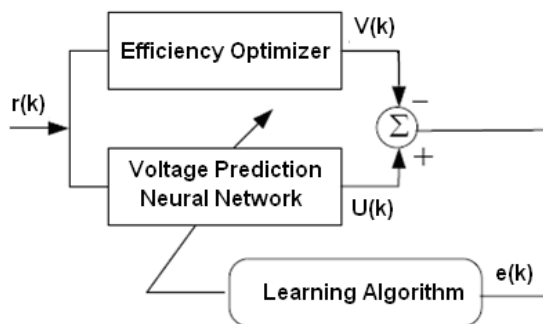


**Figure (8):** The system learning scheme for the voltage prediction neural network

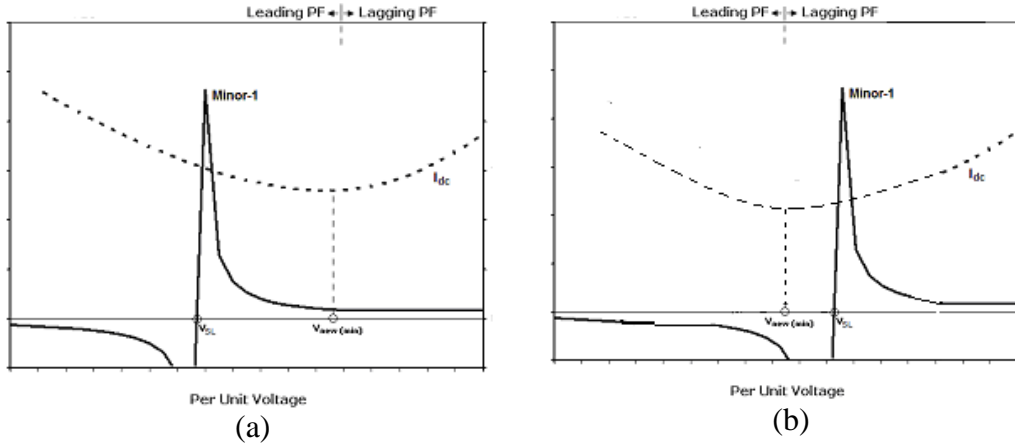


**Figure 9:** Drive Stability constraints with light- and heavy-load conditions.

The error signal drives the learning algorithm to update the feed-forward weights  $W_i$  and the base values of the hidden and output layers neurons  $b_j$  such that the performance measurement function  $E(\cdot)$  error is minimized.  $E(\cdot)$  is given by:

$$E(k) = \frac{1}{2N} \sum_{m=(k-N+1)}^k e^2(m) \tag{30}$$

where  $m$  is the current time step,  $N$  is the number that indicates the amount of past information used in the calculation of  $E(k)$ . The learning algorithm is based on the dynamic back-propagation method (Deshpande, N.A 1998). The adaptation equations for the adjustable parameters are described as follows:

$$W_i(k+1) = W_i(k) + \Delta W_i(k) \tag{31}$$

$$b_j(k+1) = b_j(k) + \Delta b_j(k) \tag{32}$$

Using the gradient descent approach (Gupta, M. 1992), the adjustments in the feed-forward parameters,  $\Delta W_i(k)$  and  $\Delta b_j(k)$ , are based on the following equations:

$$\Delta W_i(k) = -\eta_{W_i} \frac{\partial E(k)}{\partial W_i(k)} \tag{33}$$

$$\Delta b_j(k) = -\eta_{b_j} \frac{\partial E(k)}{\partial b_j(k)} \tag{34}$$

where  $\eta_{W_i}$  and  $\eta_{b_j}$  are the individual gains (learning rate) of the adaptable parameters of the neuron model, which determines the stability and speed of the convergence to the optimum values. In this study, all the values of learning rate were set to equal to 0.005.

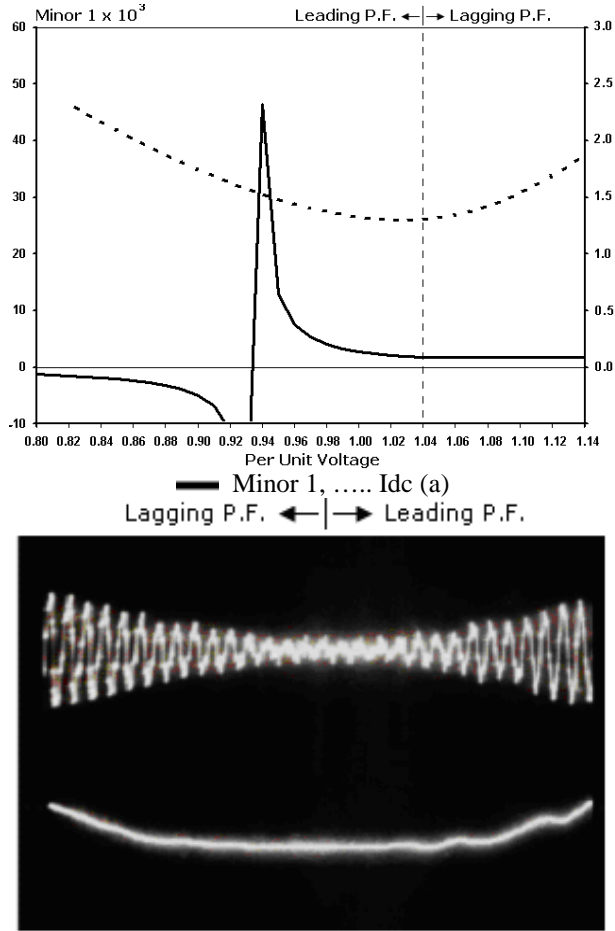
In this work, we trained the adaptive voltage prediction NN with input sequences sampled from the uniform distribution over frequency range

of (35-80Hz) in step of 5Hz and torque range (1-3N.m) in step of 0.25N.m. During the training process the system inputs are generated for the above-mentioned range where the value of the optimal per unit voltage is supplied by the iterative efficiency optimizer. During this phase the online training is performed to account for the inevitable parameter drift associated with operating conditions. Under normal operating conditions, the optimal per unit voltage is supplied by the voltage prediction network, and any drift of this voltage from the optimal value that is obtained from the iterative efficiency optimizer, correction action to the weights of the network is performed on line.

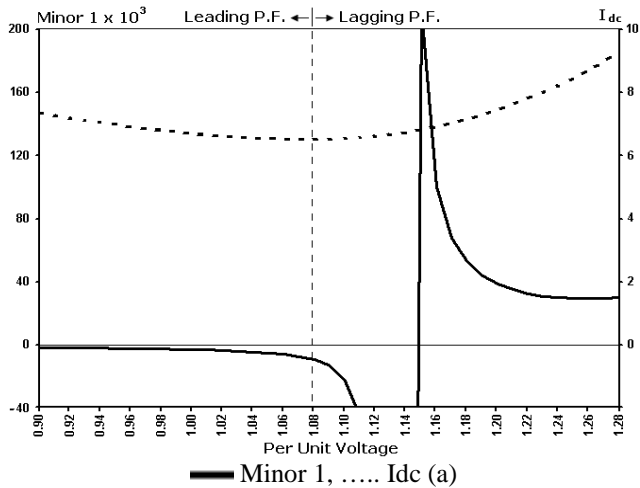
## 6. Results and Discussion

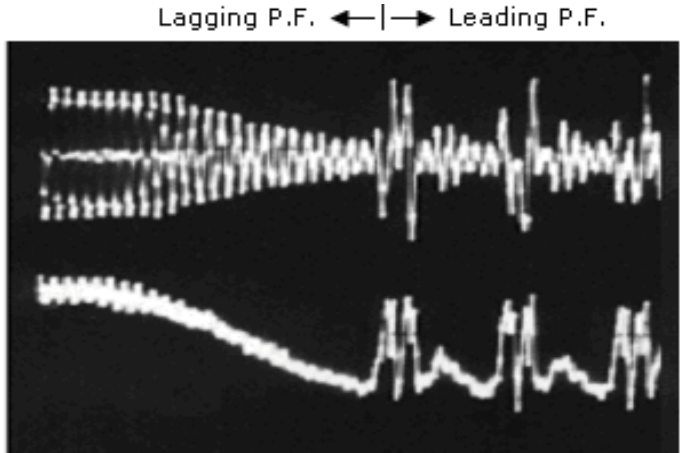
Figure 10 simulates the path of the control effort as the load torque varies from 1 – 3 N.m. with a constant supply frequency of 50 Hz. The figure also indicates that the drive system attempts to attain high efficiency. The discontinuities appear on the curves are due to the switching actions of the controller in accordance to the switchover boundaries defined by Eqn. 26.

Figures 10 and 11 compares the experimental test and predicted results for a light load and a heavy load conditions respectively. The results in these figures clearly illustrate that drive system operations with lagging, unity and leading power factors are possible with light loads and therefore the search for optimal efficiency is always successful. In contrast, with heavy load, the stability limit is shifted to a higher voltage and therefore the stable operation is only restricted to lagging power factors, as illustrated in Figure 11. For example, the maximum stability limit for a load torque of 0.5 N.m occurs at  $V_{pu} \cong 0.935$  while the stability limit for a load torque of 2.5 N.m occurs at  $V_{pu} \cong 1.15$ . This imposes a restriction on the stability margin and consequently on the maximum obtainable efficiency. The correlation between experimental and predicated results is not only demonstrated the stability margins of the drive system at light and heavy loads but also confirm validity of the stability analysis reported in Section 4. These findings are also found in correlation with the previously reported experiments and observations (Mellor, P.H. 1991) (Shimmin, D.W. 1995).



Upper: Iphase , Lower: Idc (b)  
**Figure 10:** Comparison between tested and simulated stability boundaries for a light load condition. (a) Predicated results (b) Test results

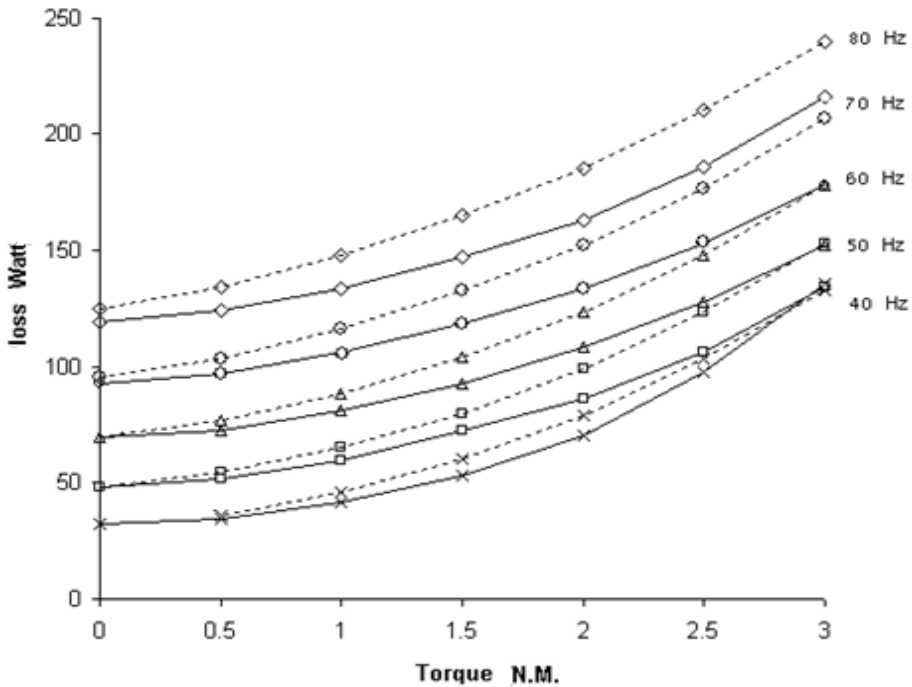




Upper: Iphase , Lower: Idc (b)

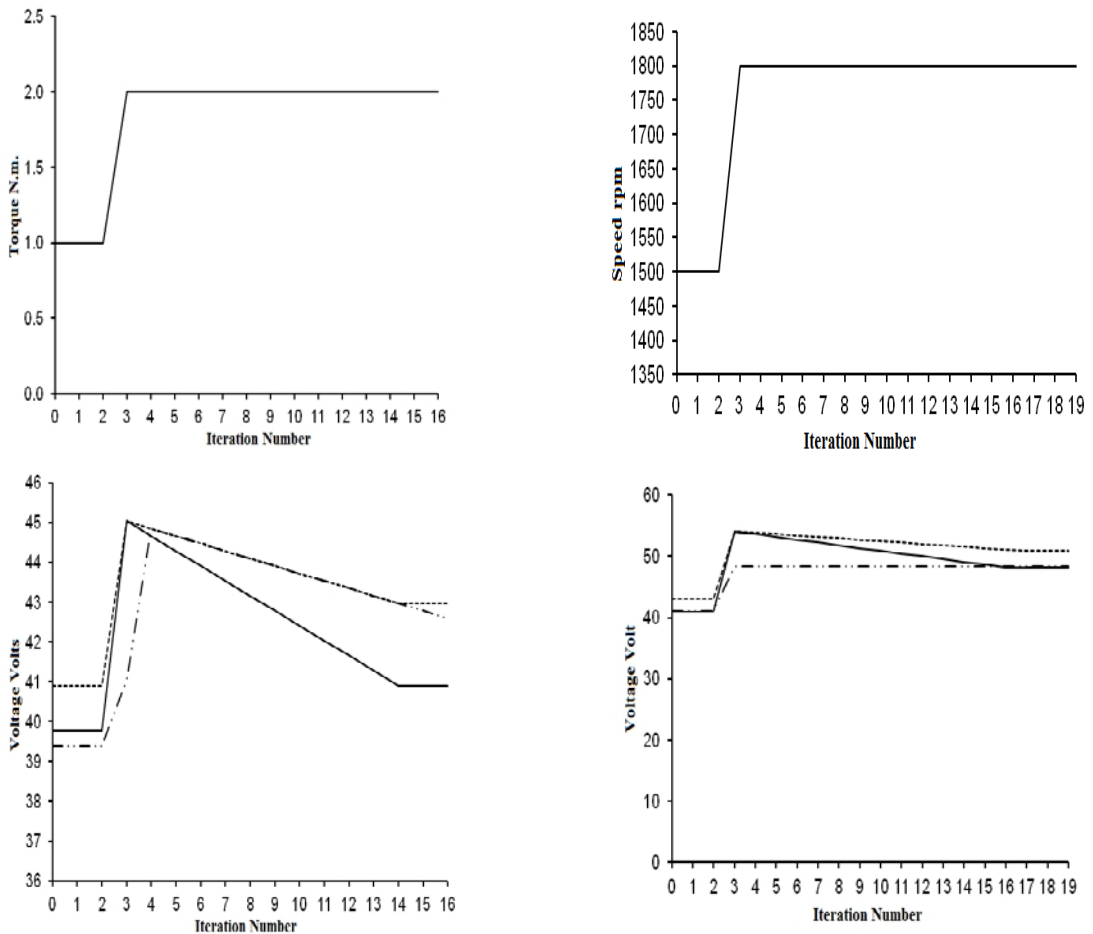
**Figure 11:** Comparison between tested and simulated stability boundaries for a heavy load condition. (a) Predicated results (b) Test results

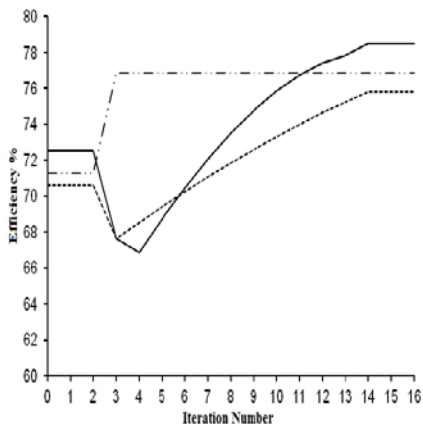
Figure 12 provides the power saving of the suggested controller against the fixed 0.9 lag power factor controller for various supply frequencies and load torques. From this figure, the power loss reduction by the proposed controller is quite obvious, especially at high frequencies.



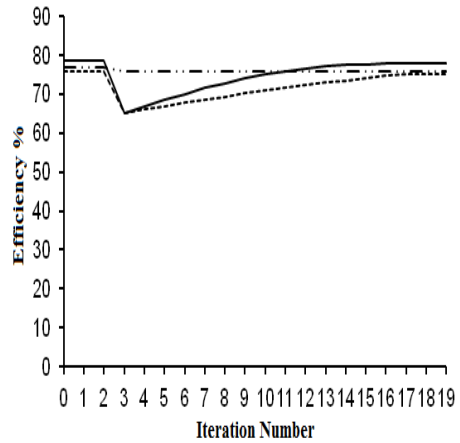
**Figure 12:** Comparison of drive power loss when operated with the fixed 0.9 lag power factor and with the proposed controller. .... Fixed 0.9 lag controller; — Proposed ANN controller

Figure 13 compares the effort of both controllers when adding and removing a load torque of 1.0 N.m. ( $\cong 33\%$  load step) to the machine at the rated frequency (50 Hz). Results in this figure demonstrate the effectiveness of the suggested controller in maintaining stable operation of the drive system when a sudden load torque is applied or removed. A similar test was carried out for step up and down in the supply frequency (i.e., speed), as shown in Figure 14. These tests also indicated that the proposed controller always attempts to attain up to 3% higher efficiency for a relatively small size motor drive when compared to that of the 0.9 lag power factor control. It should be mentioned here that the efficiency optimisation process is only applicable to the steady-state conditions. On transients in the supply frequency or the applied load, the optimisation algorithm is over-ruled and is set to overexcite the PM motor via a predefined V/F ratio in order to maintain stability.



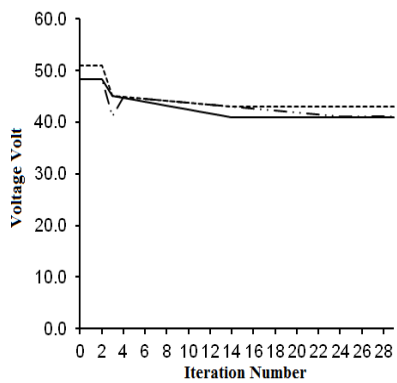
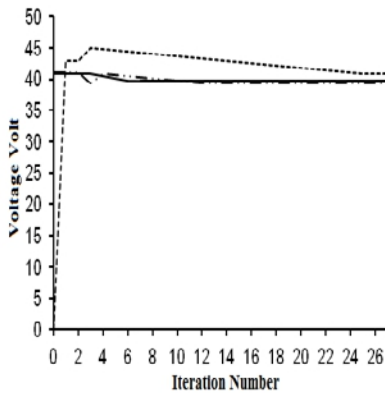
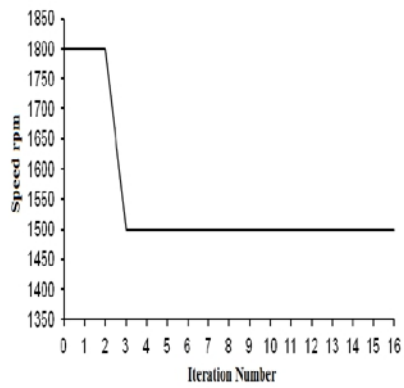
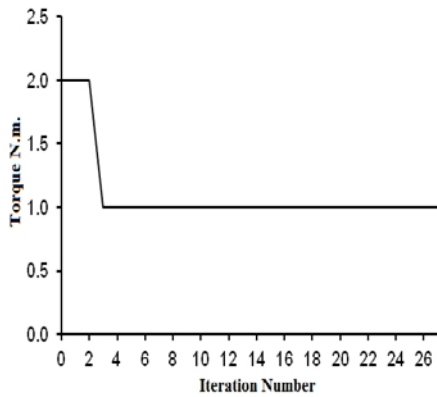


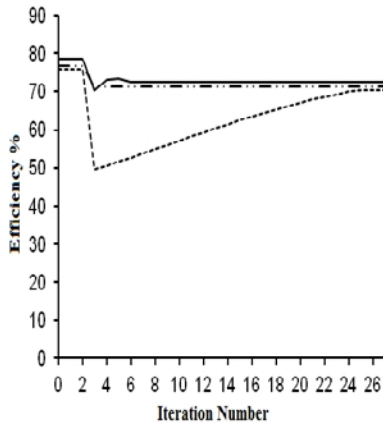
(a) Step-up input in the load torque



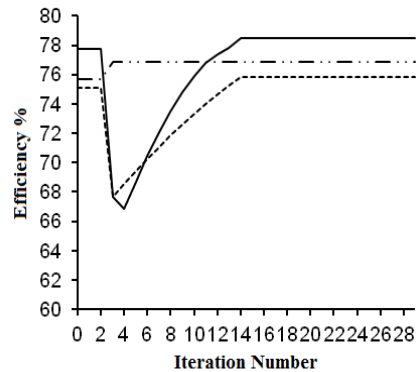
(b) Step-up input in the supply frequency

**Figure 13:** Drive system responses for step-up inputs in the applied load torque and supply frequency ...Fixed 0.9 lag controller, - · - · Stepper controller, — Proposed ANN controller





(a) Step-down input in the load torque



(b) Step-down input in the supply frequency

**Figure 14:** Drive system responses for step-down inputs in the applied load torque and supply frequency ..... Fixed 0.9 lag controller, - . - . Stepper controller, — Proposed ANN controller

## 7. Conclusion

Regions of stable operation for open loop synchronous PM motor drive system have been identified. Stability analyses based on Liapunov method, indicates that a controller based on neural network can be implemented to ensure operation at power factor values close to unity. The controller strategy always drives the system at power factors closer to unity except if the constraints specified by the calculated stability boundaries dictate otherwise. A stable and high efficiency operation can therefore be maintained irrespective of load and supply changes. Moreover, the relatively small computation time of the stability index (Minor-1) and fast NNs recognition of stability limits and maximum efficiency make it possible for real-time application of the proposed controller. The control effort of the efficiency optimisation is referenced to a single measurable variable, the DC-link current supplied to the power inverter, and thus minimizes both cost and complexity of the drive system.

## References:

- D. W. Novotny and T. A. Lipo. Vector Control and Dynamics of AC Drives. New York: Oxford Univ. Press, 1996.
- W. Leonhard: "Control of Electrical Drives. Berlin, Germany"; Springer-Verlag, 1996.
- Binns, K.J., and Wong, T.M.: 'Analysis and performance of a high-field permanent magnet synchronous machine', IEE Proc. B, 1984, 131, (6), pp. 252-258

- Faa-Jeng Lin, and Chih-Hong Lin: "A Permanent-Magnet Synchronous Motor Servo Drive Using Self-Constructing Fuzzy Neural Network Controller"; IEEE Trans. on Energy Conversion, Vol. 19(1), 2004.
- Stefan Soter, Ralf Wegener, Jens Dopheide and Bjorn Kiffer: "Low Cost Vector Control for Permanent-Magnet-Synchronmotor with only one DC-Link current Sensor for Pumping Application"; Conf. Proc. IEMDC 2005, 15-18 May 2005, San Antonio, TX, USA, 2005.
- Yong Liu, Z. Q. Zhu and David Howe: "Direct Torque Control of Brushless DC Drives With Reduced Torque Ripple"; IEEE Trans. on Industry Applications, Vol. 41, No. 2, March/April 2005.
- B. Zhang, Y. Li, and Y. Zuo, "A DSP-based fully digital PMSM servo drive using on-line self-tuning PI controller," in Proc. PIEMC 2000, vol. 2, 2000, pp. 1012–1018.
- S. R. Bowes and J. Li, "New robust adaptive control algorithm for high-performance ac drives," IEEE Trans. Ind. Electron., vol. 47, pp. 325–336, Apr. 2000.
- H. Z. Akpolat, G. M. Asher, and J. C. Clare, "A practical approach to the design of robust speed controllers for machine drives," IEEE Trans. on Industrial Electronics, vol. 47, pp. 315–324, Apr. 2000.
- S. K. Chung, J. H. Lee, J. S. Ko, and M. J. Youn, "Robust speed control of brushless direct-drive motor using integral variable structure control," Proc. IEEE Electron. Power Appl., vol. 142, no. 6, Nov. 1995.
- Perera, P. D., Blaabjerg, F., Pedersen, J. K., and Thogersen, P.: 'A sensorless, stable V/F control method for permanent-magnet synchronous motor drives', IEEE Trans. on Industrial Electronics, 2003, 39, (3), pp. 783-791.
- Al-Tae, M.A.: Stability analysis for efficiency enhancement of a high-field PM synchronous motor drive, Proc. Int. Conf. on modelling and simulation (EuroSim'04), ESIEE Paris, 6-10 September 2004.
- Al-Tae, M.A.: 'Real-time stability index for open loop controlled synchronous permanent magnet motor drive', 41st International Universities Power Engineering Conference (UPEC2006), Newcastle-UK, September 6 – 8, 2006.
- Mellor, P.H., Binns, K.J., and Al-Tae, M.: 'Ultrasonically modulated drive system incorporating PM machine', IEE Conf. Proc. on Power Electronics, London, 1988, pp. 265-268.
- Mellor, P.H., Al-Tae, M.A., and Binns, K.J.: 'Open loop stability characteristics of synchronous drive incorporating high field permanent magnet motor', IEE Proc. B, 1991, 138, (4), pp. 175-185.
- Shimmin, D.W., Wang, J., Bennett, N., and Binns, K.J.: 'Modelling and stability analysis of a permanent-magnet synchronous machine taking into account the effect of cage bars', IEE Proc. B, 1995, 142, (2), pp. 137-144.

- Yang Yi, D. Mahinda Vilathgamuwa and M. Azizur Rahman: "Implementation of an Artificial-Neural-Network-Based Real-Time Adaptive Controller for an Interior Permanent-Magnet Motor Drive"; IEEE Trans. on Industry Applications, 39(1), 2003, pp. 96-104.
- Al-Tae, M.A., Mellor, P.H., and Binns, K.J.: 'Acoustically quiet PWM inverter employing paralleled power MOSFET modules', Proc. Int. Conf. Electronics, Circuits, and Systems, IEEE Conf. (ICECS'95), 1995, pp. 146-151.
- Mellor, P.H., Chaaban, F.B., and Binns, K.J.: 'Estimation of parameters and performance of rare-earth permanent-magnet motors avoiding measurement of load angle', IEE Proc. B, 1991, 138, (6), pp. 322-330.
- Takahashi, Y., Rabins, M.J., and Auslander, D.M.: 'Control and dynamic systems', Addison-Wesley Publishing Company, 1972.
- Slotine, J.-J.E and LI, W.: 'Applied Nonlinear Control', Prentice-Hall, Inc., 1991.
- Franklin, G.F., Powell, J.D., and Emami-Naeini, A.: Feedback Control of Dynamic Systems, Addison-Wesley Publishing Company, 1994.
- Morimoto, S., Takeda, Y., Hirasaka, T. and Taniguchi, K.: 'Expansion of operating limits for permanent magnet motor by current vector control considering inverter capacity', IEEE Trans. on Industrial Applications, 1990, 26, pp. 866-871.
- Colby, R.S., and Novotny, D.W.: 'An efficiency-optimizing permanent-magnet synchronous motor drive', IEEE Trans. on Industry Applications, 1988, 24, (3), pp. 462-469.
- Mademlis, C., Kioskeridis, I. and Margaritis, N.: 'Optimal efficiency control strategy for interior permanent-magnet synchronous motor drives', IEEE Trans. on Energy Conversion, 2004, 19, (4), pp. 715-723.
- Cavallaro, C., Tommaso, A. O., Miceli, R., Raciti, A., Galluzzo, G. R. and Trapanese, M.: 'Efficiency enhancement of permanent-magnet synchronous motor drives by online loss minimization approaches', IEEE Trans. on Industrial Electronics, 2005, 52, (4), pp. 1153-1160.
- Al-Tae, M.A, Al-Azzawi, F. J, Al-Tae, A. A, and Al-Jumaily, T. Z.: Real-time assessment of power system transient stability using rate of change of kinetic energy method, IEE Proc-Gen. Trans. Distrib., 2001 148(6), pp. 505-510.
- P. Vas: "Sensorless Vector and Direct Torque Control", London, U.K.: Oxford Univ. Press, 1998.
- Deshpande, N.A, and Gupta, M.M.: Inverse kinematic neuro-control of robotic systems, Engineering Applications of Artificial Intelligence, 1998, Vol.11, No. 1, pp. 55-66.

Gupta, M. and Rao, D.: Dynamic Neural Units in the Control of Linear and Nonlinear Systems. Int. Joint Conf. on Neural Networks (IJCNN), 1992, Baltimore, pp. 100-105.

Al-Tae M.A., AlZu'bi H.S. and Al-Din M.S., Stable and highly efficient operation of open-loop controlled PM synchronous motor drive, Int. Multi-Conf. on Systems, Signals, and Devices (SSD08), Amman-Jordan. July 20-23, 2008.

### Appendix I: List of symbols

R	= Thevenin resistance of drive system, $\Omega$
$\lambda_m$	= flux linkage induced by permanent magnets, Wb
$\lambda_d, \lambda_q$	= stator d- and q-axis flux linkage, Wb
$L_d, L_q$	= stator d- and q-axis synchronous inductance, H
$\omega_s$	= stator angular frequency, rad/s
$\omega_r$	= rotor angular frequency, rad/s
p	= number of pole pairs
$T_L$	= load torque, N.m.
$\delta$	= load angle, rad
D	= motor viscous friction, kg.m <sup>2</sup> .s <sup>-1</sup>
J	= rotor inertia, kg.m <sup>2</sup>

### Appendix II: Drive System Parameters

Rated speed: 1500 r/min

Rated torque: 3.0 N.m

Number of pole pairs: 2

Rated phase voltage: 37.5 V(rms)

Rated phase current: 7.0 A(rms).

Drive Thevenin resistance: 1.26  $\Omega$

Motor core resistance: 90  $\Omega$

Motor inertia: 0.25 $\times 10^{-3}$  kg.m<sup>2</sup>

Motor viscous friction: 0.03 $\times 10^{-3}$  kg.m<sup>2</sup>.s<sup>-1</sup>

$L_{d0}$ = 3.4 mH

$K_{d1}$ = 0.06 mH/A

$K_{d2}$ = 0.31 mH/A

$L_{q0}$ = 9.2 mH

$K_q$ = 0.35 mH/A

$\lambda_{m0}$ =119 mWb

$K_e$ = 2.20 mWb/A

$I_{qe}$ = 2.0 A